Driving aggressiveness in hybrid electric vehicles: Assessing the impact of driving volatility on emission rates

Paulo Fernandes, Ricardo Tomás, Elisabete Ferreira, Behnam Bahmankhah, Margarida C. Coelho

Abstract

Hybrid electric vehicles (HEV) have demonstrated energy benefits to road traffic networks, but a deeper understanding the correlation of driving volatility with their energy use and pollutant emissions is rather rare. This paper introduces an approach based on driver volatility measured by vehicle acceleration and jerk to estimate HEV emissions rates. Dynamic emission models represented by nine driving behaviors associated with vehicular jerk classification, and considering the on/off state of the internal combustion engine are proposed. To assess real-world emission performance, data were collected from one vehicle using a portable emissions measurement system. Results indicated that proposed models using engine speed as input were good predictors of carbon dioxide and particulate matter (R^2 ranged from 0.72 to 0.96, depending on the pollutant and jerk type) for both internal combustion engine on/off states. However, the predicted emissions of nitrogen oxides resulted in values of R^2 lower than 0.57, mostly due in part to the proportion of measured concentrations lower than the instrument detection limit (~47%). Driving volatility-based models accurately characterized measured carbon dioxide (with 1–16% of measured value) and yielded lower relative mean square errors than the traditional vehicle specific power modal approach. Our results suggest that vehicular jerk classification can be useful to reduce instantaneous emission impacts during different driving regimes. For instance, these models can be integrated into electronic car units to provide feedback about emission rates associated with volatile driving and into warning systems that could detect/prevent unsafe maneuvers. These classifications would allow for better energy efficiency and eco-efficient driving behavior controls for automated vehicles.

Keywords: Hybrid electric vehicle, Driving volatility, Vehicular jerk, Carbon dioxide, Nitrogen oxides, Particulate matter

1. Introduction and research objectives

Transportation represented almost 25% of greenhouse gas (GHG) emissions in the European Union (EU) countries in 2017 [1], with road transportation accounting for over 70% of these emissions [1]. The road transportation sector also was an essential emitter of fine particulate matter ($PM_{2.5}$) and nitrogen oxides (NOx) emissions, having contributed 11% and 39% to each in 2017 [2]. Despite EU legislation restricting carbon dioxide (CO_2) emissions for new passenger cars under Regulations (EC) 443/2009 [3], the average Worldwide Harmonized Light Vehicles Test Procedure (WLTP) CO_2 for gasoline and diesel vehicles were 149.5 $g.km^{-1}$ and 152.1 $g.km^{-1}$, respectively, in 2019, which is still far from the EU target of 95 $g.km^{-1}$ for 2020 [4].

Recent statistics revealed that some consumers in the EU are opting for alternatively-powered vehicles instead of diesel vehicles [5]. In 2019, hybrid electric vehicles (HEV) represented more than 55% of alternatively-powered vehicles sold in the EU and 6% of new-car registrations [5]. Almost 900 000 units were registered during 2019, which is nearly 50% more than 2018 values [5]. It has been estimated that the sales of HEVs and other alternative-powered will reach 43 million by 2030 [6].

HEVs have less life-cycle GHG emissions, fuel consumption (FC), and, concomitantly, allow to typically attain lower tailpipe emissions compared to diesel and gasoline internal combustion engines (ICE) [6], [7]. The improved energetic and environmental benefits of HEVs are due to their operating system that consists of an ICE assisted by an electric device to propel the vehicle and a battery to store the energy produced either by the ICE or by regenerative braking [8]. However, HEVs produce sporadic high emissions when the ICE is restarting, which results from a combination of circumstances such as: driving conditions, vehicle speed, road grade, ambient temperature, driver aggressiveness, and HEV system design [9], [10]. Moreover, frequent restarts mean longer warming up periods for HEVs that can significantly increase FC and exhaust emissions until the ICE and after treatment are fully warmed [10].

Currently, there are four types of HEV powertrain configurations: parallel, series, power-split or series-parallel hybrid, and multi-mode [11]. In the parallel hybrid configuration, both the engine and electric motors can individually or jointly operate as the power source. Usually, the engine operates as the most dominant power-source while the electric motor engages for assistance. In the series hybrid, only the electric motor runs the drivetrain. Since the engine is not mechanically coupled to the drivetrain, it can consistently operate at its most efficient speed and work as a generator to power the electric motor or to recharge the batteries. The power-split (or series-parallel hybrid) allows the vehicle to operate either in parallel or series, thus achieving higher operational efficiencies. The multi-mode hybrid powertrain consists of adding clutches to parallel or power-split powertrain systems, which can become any of the above-mentioned hybrid configurations in the same powertrain [11].

Despite the environmental benefits, there is a need for a full understanding of instantaneous behavior using a driving volatility analysis for both HEV energy use and pollutant emissions. This paper introduces an approach based on driver volatility measured by vehicle acceleration and jerk to estimate HEV emissions rates. Therefore, the specific objectives include:

(1) To examine the influence of speed, acceleration, vehicular jerk, RPM, and grade on HEV emission rates;

(2) To develop second-by-second CO_2, NOx, and Particulate Matter (PM) hot emissions for a selected HEV that account for driving volatility as a means of vehicular jerk classification;

(3) To compare the HEV emission model based on driving volatility and a vehicle specific power (VSP) modal emission approach.

The findings from this paper can be beneficial in three ways. Firstly, the definition of nine driving types based on vehicular acceleration and jerk classification that covers driving types that are important from a safety point for an on-road vehicle, regardless of the site-specific operational conditions. Secondly, the driving volatility information can be used in HEV warning systems to alert the driver about behaviors associated with high fuel consumption levels and unsafe maneuvers. This last point is especially critical since driving volatility represents a safety concern not only in HEVs but also in other types of vehicles. These warnings can reduce driving volatility, thereby assisting vehicle engineers in designing more energy-efficient driving behavior controls for the autonomous vehicles, in particular powered by the HEV technology. Thirdly, the estimation of emissions using vehicular jerk classification can be incorporated into electronic control units (ECUs) to provide feedback about emission rates based on driving style. Although the models were developed using one probe car, the methodology is replicable to all vehicle types by simply knowing vehicle jerk type, and correlating engine parameters and emission rates.

2. Literature review

Portable Emissions Measurement System (PEMS) devices make feasible the correlation of driving conditions and engine and vehicle operating parameters with related exhaust emissions, as they record on-board measurements of tailpipe emissions at a high-resolution time [12]. Emission measurements studies have been conducted for HEVs using PEMS, as presented in Table 1. Some work has been conducted on VSP [13], ambient temperatures [14] and battery states of charge [15], [16] impacts on emission values. Zhai et al. [13] conducted a study on a 2001 Toyota Prius and reported increases in CO_2 (0.5–5 $g.s^{-1}$), and carbon monoxide (CO) (<1–20 $mg.s^{-1}$) for VSP from less than −2 to 19 $kW.ton^{-1}$, but that study did not include data values where the ICE engine was always on (VSP > 19 $kW.ton^{-1}$). Alvarez and

Weilenmann [14] studied the influence of low ambient temperature on HEV FC and CO_2 emissions for five HEVs models. The results show that the amount of HEV cold-start extra emissions were on average 30–85% lower than cold-start extra emissions of conventional gasoline vehicles. Moreover, the HEV cold-start extra emissions of FC and CO_2 were similar to those of conventional gasoline-fueled vehicles, except at an ambient temperature of 23 °C. Duarte et al. [16] confirmed that an ICE on period longer than 30 s led to increases in NOx fuel-based emissions up to 73% on a full HEV. Also, battery state of charge (SOC) affected the amount of time the ICE was off, such that lower SOC levels (40–50%) resulted in higher NOx emissions.

Table 1
Key studies on HEV emissions using PEMS.

Reference	Year	Vehicles Tested	Study Focus	Main Parameters	Observations
[13]	2011	Toyota Prius (model year –2001)	To quantify ICE on/off operation rules and develop an exhaust emissions model under hot stabilized conditions	CO_2, CO, NOx, HC, RPM	Emission model only based on VSP and RPM combination; PM not analyzed; Influence of vehicular jerk on emissions not considered.
[14]	2012	Five HEVs (model years ranged from 2005 to 2009)	To examine the influence of low ambient temperature on fuel consumption and pollutant emissions	CO_2, CO, NOx, HC, FC	Measurements performed in urban conditions; PM not analyzed; Influence of vehicular jerk on emissions not considered.
[15]	2010	Three HEVs (model years ranged from 2005 to 2006)	To analyze the effect of hybrid system battery performance on CO_2 emissions	CO_2 per unit distance	Tests conducted in a wide range of road types at constant speed with full electric driving and vehicle traction modes; NOx and PM were discarded; Influence of vehicular jerk on emissions not considered.
[16]	2014	Toyota Prius (model year –2011)	To analyze the effect of SOC in the fuel consumption and pollutant emissions	FC, CO_2, CO, NOx	Energy and environmental characterization combined on-road measurements with VSP; PM not analyzed; Influence of vehicular jerk on emissions not considered.
[17]	2015	Toyota Camry (model year – 2010)	To compare emissions and fuel consumption rates of a HEV and its CV counterpart	CO_2, fuel consumption rate (FCR)	HEV benefit (ratio of the mean CV CO_2/FCR to the mean HEV CO_2/CV) was computed from VSP; NOx and PM were discarded; Influence of vehicular jerk on emissions not considered.
[18]	2015	Two Toyota Prius (model years – 2007 and 2010)	To measure on-road emissions and fuel consumption values and compare HEV benefits in relation to ICE (gasoline and diesel)	Total Hydrocarbons (THC), NOx, CO, CO_2	PM not analyzed; Influence of vehicular jerk on emissions not considered.
[19]	2018	Two HEVs (model years – 2015)	To compare emissions and fuel consumption rates of an HEV and its CV counterpart	CO_2, CO, Oxygen (O_2), HC and NO	PM not analyzed; Influence of vehicular jerk on emissions not considered.
[20]	2015	Toyota Camry (model year – 2010)	To quantify the magnitude of particulate number from reignition events and understand the differences between ICE operation and particulate number across three roadway types	Particulate number emission rates (PNER), RPM	Energy and environmental characterization combined on-road measurements with VSP; Influence of vehicular jerk on emissions not considered.
[21]	2020	Toyota Prius (model year – 2013)	To develop a method for quantifying the real-world activity, energy use, and emissions of a plug-in hybrid electric vehicle based on charge depleting or charge sustaining mode	CO_2, NOx, HC, Fine Particulate Matter (PM2.5)	Influence of vehicular jerk on emissions not considered.
[22]	2020	Toyota Camry (model year – 2010)	To examine the relationships between instantaneous hybridization factor, VSP, real-world road type and road grade.	Particulate Number, CO_2, FCR	NOx were discarded; Influence of vehicular jerk on emissions not considered.

Previous studies have quantified emissions and FC benefits differences between HEVs and ICEs. Holmén and Sentoff [17] compared one HEV and its counterpart conventional vehicle on the same route with the same driving profile. They concluded that HEV benefits decrease for higher average speed rural and freeway driving. Wu et al. [18] have found average CO_2 emissions reductions from two Euro 5 Toyota Prius gasoline-electric vehicles by approximately 35% and 15% relative to conventional gasoline and diesel cars, respectively, in Macao. Huang et al. [19] examined two identical model CV/HEV passenger car pairs on three test routes, where HEVs showed an on-road 23–49% FC benefit compared to the CVs. However, the HEVs showed high nitrogen monoxides (NO), CO and hydrocarbon (HC) emission events observed during short periods due to the lower HEV three-way catalyst effectiveness when the ICE is off.

The effects of HEV ICE on-off cycles in low speed situations have negative impacts on particulate number (PN) emission rates. Conger and Holmén [20] indicated that during urban and rural driving, 59% and 45% of all HEV high-emission events, respectively, occur as a result of engine reignitions. Recently, Frey et al. [21] investigated the main sources of variability in terms of emission rates and energy use for a plug-in hybrid electric vehicle (PHEV). They considered the power demand, charging model, cold-start and hot-stabilized operation, and electricity generation resource mix. Although results confirmed both energy and emission benefits for PHEVs over conventional light duty vehicles, the PHEV was sensitive to the above-mentioned factors and produced high on-road emissions rates during cold starts.

Although road grade is an important factor in quantifying exhaust emissions accurately, few studies have addressed in detail real-world road grade impacts on HEV emissions. For instance, Robinson and Holmén [22] studied a relationship between instantaneous hybridization factor (ratio of electric system power to total system power that accounts for energy storage in the high voltage battery), VSP and real-world road grade. They developed a CO_2 model using a VSP computed with real-world road grade that provided an improved fit (R^2 = 0.87) over the no-grade VSP model (R^2 = 0.6).

Prior studies have demonstrated that high fuel consumption (FC) is associated with aggressive driving behavior, for instance, extreme braking and speed-ups [9]. It must be stressed that during real driving conditions, the traffic environment along the road can be rather complex. For instance, a vehicle's non-compliance with a yield signal on a secondary road or unexpected pedestrians crossing road far from crosswalk can result in sudden accelerations and decelerations during a trip. Vehicular jerk can represent the temporal dynamics of the acceleration and deceleration of a vehicle. Vehicular jerk, which is defined as the rate at which an object's acceleration changes with respect to time, can be used as an indicator of driving volatility [23], thus, it is an aggregate measure of driving performance.

Earlier studies of HEVs have used speed and acceleration to measure driving aggressiveness and FC [24], [25], but the available on-road HEV data needed to assess the impacts of vehicular jerk on energy use [26], [27] and hot-stabilized emissions are scarce. In a recent study by Rio-Torres et al. [27], three different driving styles (normal, calm, and volatile) were used to quantify possible improvements in FC. The HEV FC savings reached 12% and 4% for normal urban and normal highway driving, respectively [27].

Other authors conducted a jerk-based analysis on emissions for a broad range of topics, such as interactions between motor vehicles and cyclists at urban multi-lane roundabouts [28], development of dynamic FC models [29], spatial distributions of jerk, and CO_2 and NOx emissions in different roundabout layouts [30], however, their research was only applied to ICEs.

The literature review revealed that each of the prior studies had shortcomings that do not enable full characterization of HEV emissions and driving volatility. These shortcomings included the influence of driver volatility in HEV on-road emissions using vehicular jerk, as well as the development of HEV emission models for both global and local pollutants that consider driving behavior styles based on vehicular jerk. This paper fills these gaps through the establishment of a full understanding of HEVs in terms of on-road emissions, engine data, and driving volatility in real-world driving conditions. The further integration of driving volatility and emissions rate information to optimize road vehicle performance, in particular for HEVs, is worthy of research at this stage. This study is unique since it uses driving volatility analysis to assess tailpipe emissions of an actual HEV, and it establishes a jerk classification based on cruise and volatile states, internal combustion engine status, and engine parameters to predict both global (CO_2) and local (NOx and PM) pollutant emissions.

3. Methodology

The methodology was applied for real-world data collected from one model and make of a HEV tested under different driving conditions. It proceeded in four main sections: study experimental design (Section 3.1), equipment (Section 3.2), data processing and quality assurance (Section 3.3), and data analysis (Section 3.4).

3.1. Study design for field measurements

Second-by-second on-road emissions, engine, and Global Positioning System (GPS) data were collected on three routes in the Aveiro region in Portugal (see Fig. S1). The routes were designed to include urban, extra-urban and highway roads, and different road grades [31], [32] and they were based on one origin–destination pair with three alternatives, as follows: i) R1 includes 5.5 km and 18.1 km on urban and extra-urban arterials, respectively; ii) R2 has 7.4 km and 22.8 km along extra-urban arterials and highways (including entry/exit ramps), respectively; and iii) R3 includes 12.8 km and 23.7 km in extra-urban arterials and highways (including entry/exit ramps), respectively. Traffic volumes at R3 are typically four times more than R2 values [31]. The speed limits on the studied routes are encompassed between 40 and 50 $km.h^{-1}$ for urban roads, 50–70 $km.h^{-1}$ for extra-urban, and 120 $km.h^{-1}$ for highways. Fig. 1 depicts the

grade profile in each 100-m road segment on the three routes by travelling direction. The road grade for 40%, 30% and 40% of the R1, R2 and R3 length, respectively, ranges from −1% to 2%, while the number of segments with positive grades are as follows: a) 64 (~54%) in R1 South-North; b) 51 (~44%) in R1 North-South; c) 87 (~60%) in R2 South-North; d) 60 (~41%) in R2 North-South; e) 87 (~52%) in R3 South-North; and f) 79 (~47%) in R3 North-South.

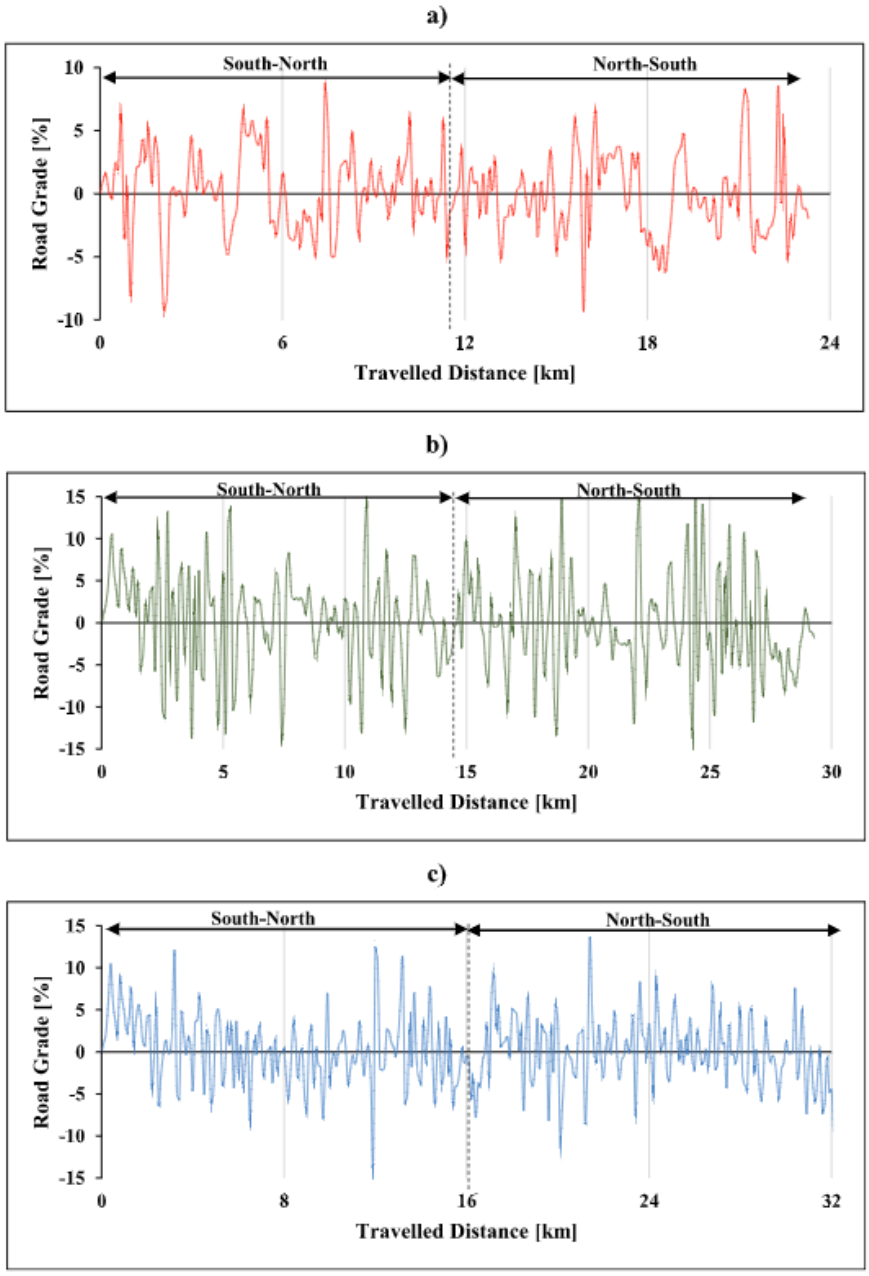

Fig. 1. Road grade profile in each 100-m segment: a) R1; b) R2 and c) R3.

The tested vehicle was a 2019 Toyota full HEV model combining a 2ZR-FXE Atkinson-cycle 1.8L gasoline ICE with an electric motor through a multi-mode power-split powertrain [20]. Table 2 presents the ICE, environmental, emission, and performance characteristics of the vehicle. Two drivers drove the testing vehicle along the described routes. Collected data covered approximately 17 000 s (nearly 5 h) and almost 280 km of road. The average temperatures observed during monitoring campaigns ranged from 15 °C and 17 °C, while humidity ranged between 60% and 75%.

Table 2. Summary of the characteristics of the testing vehicle.

Specification	Toyota C-HR 1.8 Hybrid
Fuel	Gasoline
Mileage (km)	7,500
Transmission	Continuously variable transmission automatic gearbox
Engine	1.8-Liter 4-Cylinder
ICE compression ratio	13:1
ICE power (kW/RPM)	90/5,200
ICE torque (Nm)	142
Electric motor type	Permanent Magnet AC
Electric motor (kW)	53
Electric motor torque (Nm)	180
Battery type	Lithium-ion
Battery capacity (Ah)	3.6
Battery nominal voltage (V)	207.2
Vehicle gross mass (kg)	1,860
Maximum Speed ($km.h^{-1}$)	170
Combined WLTP CO_2 ($g.km^{-1}$)	87
Combined Fuel Consumption ($L.100\ km^{-1}$)	3.9

3.2. Equipment

Tailpipe emissions concentrations were measured using a 3DATX ParSYNC integrated PEMS (iPEMS) [33]. The instrument measures the volume fraction of CO_2, NO, and nitrogen dioxide (NO_2) on a second-by-second basis using consumable GasMOD™ Sensor Cartridges. Since NOx emissions are approximately 95% of NO and 5% of NO2 for gasoline vehicles, NO is used as surrogate for NOx [34]. This iPEMS uses three detection methods to measure PM based on opacity, ionization and light-scattering, which are sensitive to PM size fractions in the coarse PM (approximately 2.5 µm to over 10 µm), fine PM (0.3–2.5 µm) and ultra-fine PM (up to 0.4–0.5 µm) modes, respectively. Each detector indicates a voltage, which is subtracted from a reference value reported before each test [33]. Quality control procedures involved routine calibration checks using a UN 1956 gas mixture and the execution of a warm-up route of 30 min to assure the vehicle was under hot stabilized operation during the measurements. Table S1 presents more details concerning the range, sensitivity, and resolution of the iPEMS sensors.

An ELM327 on-board diagnostics (OBD) tool reported second-by-second ICE data, as follows: i) OBD speed; ii) engine revolutions per minute – RPM; iii) engine load; iv) fuel flow rate – FFR; v) mass air flow – MAF; and vi) intake air temperature – IAT. OBD also provided the air-to-fuel ratio (AFR) and the engine volumetric efficiency (ηengine). Garmin GPS receivers recorded latitude, longitude, and altitude. A linear regression of altitude versus distance was used to estimate road grade for sequential 100-m segments of each trip [35], and using the corrected instantaneous vehicle altitude data, as described elsewhere [36].

3.3. Data processing and quality assurance

Time alignment of iPEMS, OBD and GNSS signals was done prior to doing the emissions calculations following a method described here [34], [37]. This alignment was based on engine parameters using engine speed reported by the ECU. For each pair of data sets to be synchronized, an indicator variable exhibiting concurrent trends (e.g., rise in engine speed and concordant rise in concentration of exhaust gas) was used. To assess the quality of synchronization, the Pearson Correlation Coefficient (PCC) measured the linear statistical dependence between engine RPM and iPEMS NOx (as suggested for Light Duty Vehicles [34]) using NOx volumetric concentration as the primary indicator variable and RPM as the secondary indicator variable. Figs. S2-S4 exhibit time series plots before and after synchronization and PCC values by each set of measurement, i.e., every time the iPEMS was started. A correct synchronization between x-axis and y-axis was achieved after adjusting RPM time stamps by +2, −8 and +5 s in sets 1, 2

and 3, respectively. The maximum PCC values ranged from 0.35 and 0.65, which signifies that data sets were well-synchronized [34].

Erroneous data were checked by taking into account quality assurance screening criteria [34], [37], along with the synchronization of data from all equipment into one database. The most typically errors included unusual AFR values, constant engine values, concentrations lower than zero or conditions where external factors (e.g., temperature) were found to affect sensors outputs. AFR values can be erroneous due to air leaks into the sampling line. Constant OBD values mean that data was no longer being updated during short periods (usually between 5 and 10 s). Negative concentrations occurred more often with NOx and represented low values that are not statistically different from zero. These negative concentration values were zeroed for data analysis.

3.4. Data analysis

3.4.1. Verification of trips

The criteria in the Real Driving Emissions (RDE) procedure, which is based on the ninety-five percentile of the product of 1 Hz of vehicle speed and positive accelerations higher than 0.1 m/s^2 (here denoted as vapos_[95]), and relative positive acceleration (RPA) metrics, were applied to validate PEMS trips [36]. The verification analysis confirmed that all trips fulfilled the RDE criteria, as depicted in Fig. S3.

3.4.2. Emission rates

The method described by Regulatory Information 40 CFR 86.144 was used to compute mass per-time exhaust emissions [38]. It uses engine MAF and AFR reported via the OBD [34]. Supplementary Materials provides full details concerning the calculations of mass per time-based tailpipe emission rates. The method for computing PM mass emission rates from the voltages of the scattering, ionization, and opacity sensors is also provided.

Almost every driving behavior can be characterized as calm or volatile. While calm driving can be characterized as maintaining speed without high accelerations or decelerations, volatile driving can have a negative impact on emissions generated by vehicles. For volatile driving behaviors, vehicular jerk can be defined as the instantaneous change of driving acceleration within two seconds, as follows [27]:

$$j = \frac{da}{dt} = \frac{d^2v}{dt} \quad (1)$$

where j is the vehicular jerk (m.s^{-3}), v is the vehicle speed (m.s^{-1}), and a is the acceleration (m.s^{-2}).

Having in mind that jerk expresses how a driver changes acceleration and deceleration rates by adjusting pressure on the pedals, Zhang et al. [29] defined nine jerk types to represent volatile and cruise states at each sampling speed, as presented in Table 3.

Table 3. Driver behavior classification based on jerk [29]

Driver behavior classification based on jerk [29]

Type	Description	Expression
1	maintaining acceleration	$a_t > 0 \,\&\, a_{t+1} > 0 \,\&\, a_t - a_{t+1} \to j - 0$
2	maintaining acceleration	$a_t > 0 \,\&\, a_{t+1} > 0 \,\&\, a_t > a_{t+1} \to j < 0$
3	maintaining acceleration	$a_t > -0 \,\&\, a_{t+1} > 0 \,\&\, a_t < a_{t+1} \to j > 0$
4	maintaining deceleration	$a_t < 0 \,\&\, a_{t+1} < 0 \,\&\, a_t - a_{t+1} \to j - 0$
5	maintaining deceleration	$a_t < 0 \,\&\, a_{t+1} < 0 \,\&\, a_t < a_{t+1} \to j > 0$
6	maintaining deceleration	$a_t < -0 \,\&\, a_{t+1} < 0 \,\&\, a_t > a_{t+1} \to j < 0$
7	alternate accelerating and decelerating	$a_t > 0 \,\&\, a_{t+1} < 0 \,\&\, a_t > a_{t+1} \to j < 0$
8	alternate accelerating and decelerating	$a_t > 0 \,\&\, a_{t+1} < 0 \,\&\, a_t < a_{t+1} \to j > 0$
9	cruise speed	$a_{t+1} - 0 \,(a_t - 0)$

It must be stressed that cruise states can account for a large proportion of total jerk and emissions on a trip. For this reason, a model in the form of Eqs. (2), (3), (4) was used:

$$E_{jerk,g} = E_{cruise,g} + E_{volatile,g}, \quad (2)$$

$$E_{cruise,g} = \sum_{h=1}^{N_h} e_{jerk9,h,g}, \quad (3)$$

$$E_{volatile,g} = \sum_{m=1}^{8} \sum_{w=1}^{N_w} e_{w,m,g}, \quad (4)$$

where is the predicted trip emissions based on vehicular jerk of specie g (g), is the amount of emissions of specie during the cruise state (g), is the amount of emissions of specie g during volatile states represented by jerk types 1 to 8 (g), Nh is the number of seconds in jerk type 9, is the emission rate ($g.s^{-1}$) in the second of travel h and specie g, m is the index of jerk type, , is the number of seconds in jerk type m; and is the emission rate ($g.s^{-1}$) in the second of travel w, jerk type m and specie g.

The emission rates by jerk type can be represented as a function of vehicle speed or specific internally observable variables (IOVs), such as RPM [39]. Thus, the relationship between CO_2, NOx and PM and these variables and with different ICE operation rules was explored.

4. Results

The results section includes a summary of experimental results (Section 4.1), engine on-off operation rules (Section 4.2), exploratory data analysis (Section 4.3), empirical driving volatility-based emission models (Section 4.4) and comparative performance between VSP and driving volatility based approaches (Section 4.5). The Supplementary Materials contain more details concerning routes, quality assurance, experimental measurements, jerk types by route, cycle emission rates and the relationship between jerk types and emissions.

4.1. Summary of experimental results

4.1.1. Driving behavior

To explore the influence of the two drivers in acceleration and jerk distributions, a two-sample Kolmogorov- Sminorv test (K–S test) for 90% and 95% confidence levels was applied. The plots in Fig. 2 show the acceleration and jerk distributions in terms of cumulative distributions on three routes. It can be verified that both acceleration and jerk distributions followed the same trends for both drivers, regardless of the confidence level. For example, the two-sample K–S test (D-value) results with a 95% confidence level for acceleration distributions were 0.025 (D-critical = 0.026), 0.036 (D-critical = 0.047) and 0.038 (D-critical = 0.062) for R1, R2 and R3, respectively. For jerk, the distributions of both drivers in all routes did not exhibit significant differences. Therefore, the data from both drivers as one was used in the development of driving volatility-based models in this paper.

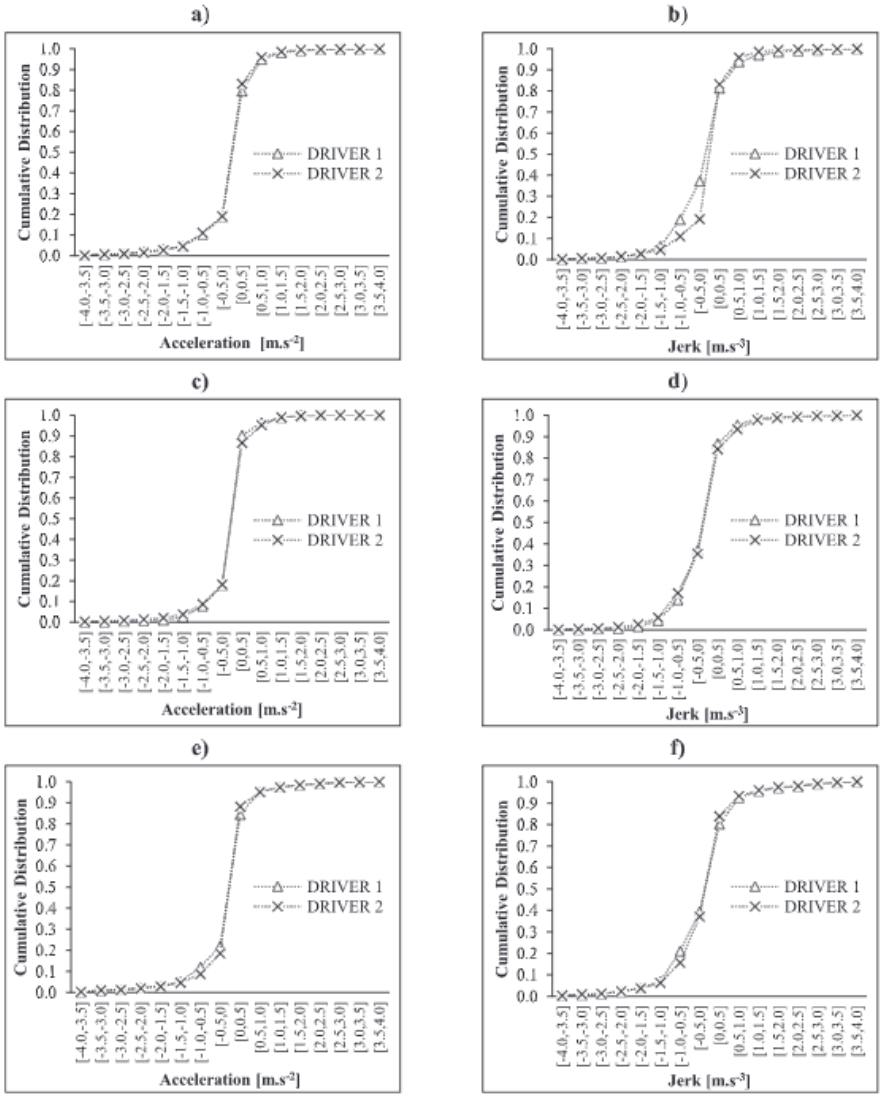

Fig. 2. Influence of drivers on performance measures: a) Acceleration – R1; b) Jerk – R1; c) Acceleration – R2; d) Jerk – R2; e) Acceleration – R3; and f) Jerk – R3. Note: The null hypothesis (H0) is that samples come from the same distribution. If D-value > D-critical, then H0 is rejected.

4.1.2. HEV operation

To understand the difference in HEV operation by route, a graphical comparison of OBD speed, slope (computed in each 100-m road segment as suggested in [35]), RPM, FFR, VSP and vehicular jerk is depicted in Fig. 3 for a 20 km subset comprising R1 and partially R2. The x-axis represents vehicle locations (in kilometers from the beginning of the R1), and vertical dotted lines indicate the location of traffic singularities. The plots indicated that both engine speeds and FFR widely varied across R1 because of the HEV ICE on-off operation rules. For instance, FFR was zero for approximately 50% of the R1 trip time, which means that the ICE was not used. Most of the reignition events for R1 occurred during acceleration due to traffic control or on positive slopes. However, this fact did not hold for R2, where RPM and FFR did not reach 0. It can be also noted that negative or low VSP values are found for many events with engine speeds of 0 RPM, which are associated with reignition events in urban areas where the vehicle is either in a stop-and-go situation or is accelerating at low speeds causing cyclical on/off states of the ICE. For vehicular jerk, a different pattern between R1 and R2 was observed. While vehicular jerk had considerable variations across R1 (perhaps due to the presence of intersections, speed bumps or pedestrians crossing

the road that resulted in sharp accelerations or decelerations), its range of values was much lower across R2 (between −2 $m.s^{-3}$ and 2 $m.s^{-3}$).

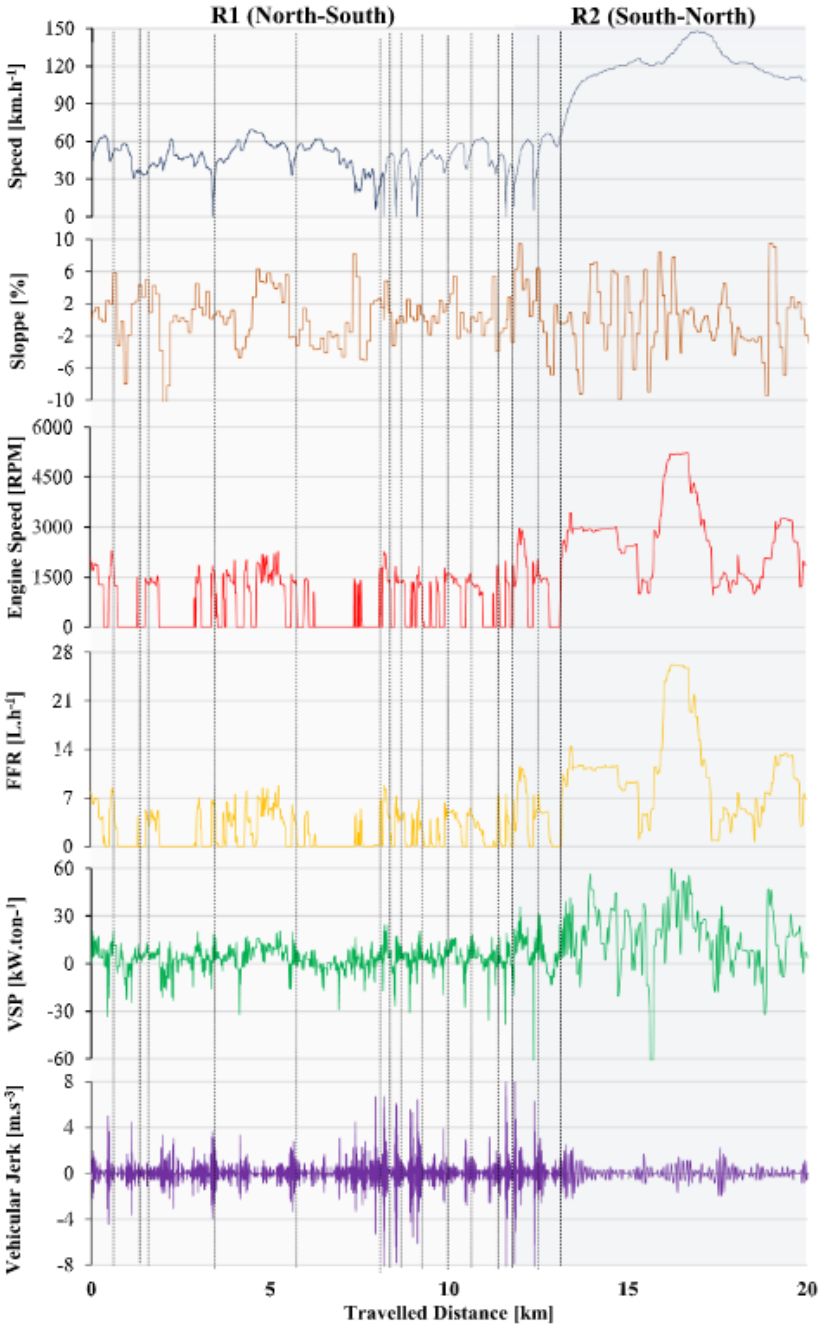

Fig. 3. Example of a driving route vehicle speed, slope, engine speed, FFR, VSP and vehicular jerk.

4.1.3. Route emissions

Following previous results, and as expected, CO_2 emissions (mean $g.km^{-1}$ ± standard deviation values) were on average lower for R1 (65 ± 5 $g.km^{-1}$) than the R2 (142 ± 13 $g.km^{-1}$) and R3 (114 ± 10 $g.km^{-1}$), as shown in Fig. 4. R2 achieved higher energy use and exhaust emissions for two main reasons. First, there is a higher variability in road grade compared to R1 and R3 (see Fig. S6). While the range of road slopes from 2% to 11% represent less than 10% of R1 and R3 length, these uphill roads account for more than

22% of R2 length. Second, vehicles drove at higher speeds for R2 than R3 (perhaps due to low traffic volumes), as it can be seen in Fig. S7, where a higher occurrence of speeds over 100 km/h can be found for R2. The findings for fuel consumption followed an identical trend because more than 99% of CO_2 resulted from the carbon in the fuel [40]. The average R1-trip fuel consumption was approximately 54% and 42% lower than R2 and R3, respectively. It was found that the trip values yielded CO_2 (97 ± 16 g.km^{-1}) and fuel consumption (4.2 ± 0.7 L.100 km^{-1}) close to the vehicle type-approval values (see Table 2 for those details). From Fig. 4, it can be also observed greater variability in NOx than PM values, regardless of the studied route; the ratio of the standard deviation to the mean (coefficient of variability – CV) of NOx was 0.4, 2.3 and 0.9 in R1, R2 and R2, respectively, while for PM the resulting CV values were lower than 0.3 in all routes. Despite the higher variability, the differences in the NOx emissions per kilometer in average per trip between the highway routes were not statistically significant (p-value < 0.05).

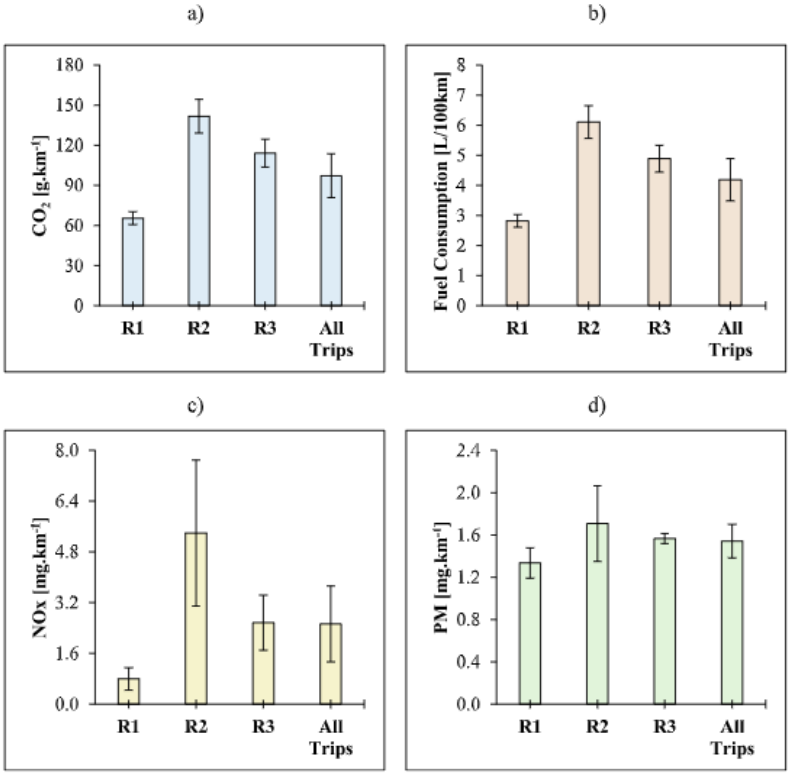

Fig. 4. HEV energy and emissions performance by route (with standard deviation values): a) CO_2 per kilometer; b) FC; c) NOx per kilometer; and d) PM per kilometer.

It is worth to notice that the high range of HEV NOx values is mostly due to spikes during fuel injection after fuel cut, especially during low-speed and sudden heavy-load conditions, which are prone to induce instances where the engine runs under lean mixture [41]. These operation conditions translates into a lower capability from the engine to develop a cooler combustion from which results NOx emissions spikes. To demonstrate this, Fig. 5a exhibits two engine restarts in a subset of one trip from R1 (average NOx ≈ 0.93 mg.km^{-1}) at a higher engine load operating under lean fuel mixture ($\lambda > 1.0$). The high concentration levels combined with high exhaust mass flow rates during acceleration generated increases in NOx emissions per unit distance 55–75 times higher than the average trip value. Fig. 5b and c show another two spikes in mass NOx during heavy-load conditions on a subset of R2 (average NOx ≈ 3.4 mg.km^{-1}) and R3 (average NOx ≈ 3.2 mg.km^{-1}) trips. The increases in NOx emissions were found to be perceptible in both cases (16–55 times and 30–40 times higher than the R2 and R3 average values, respectively). Other trips also recorded these spikes in NOx emission rates when the ICE restarts.

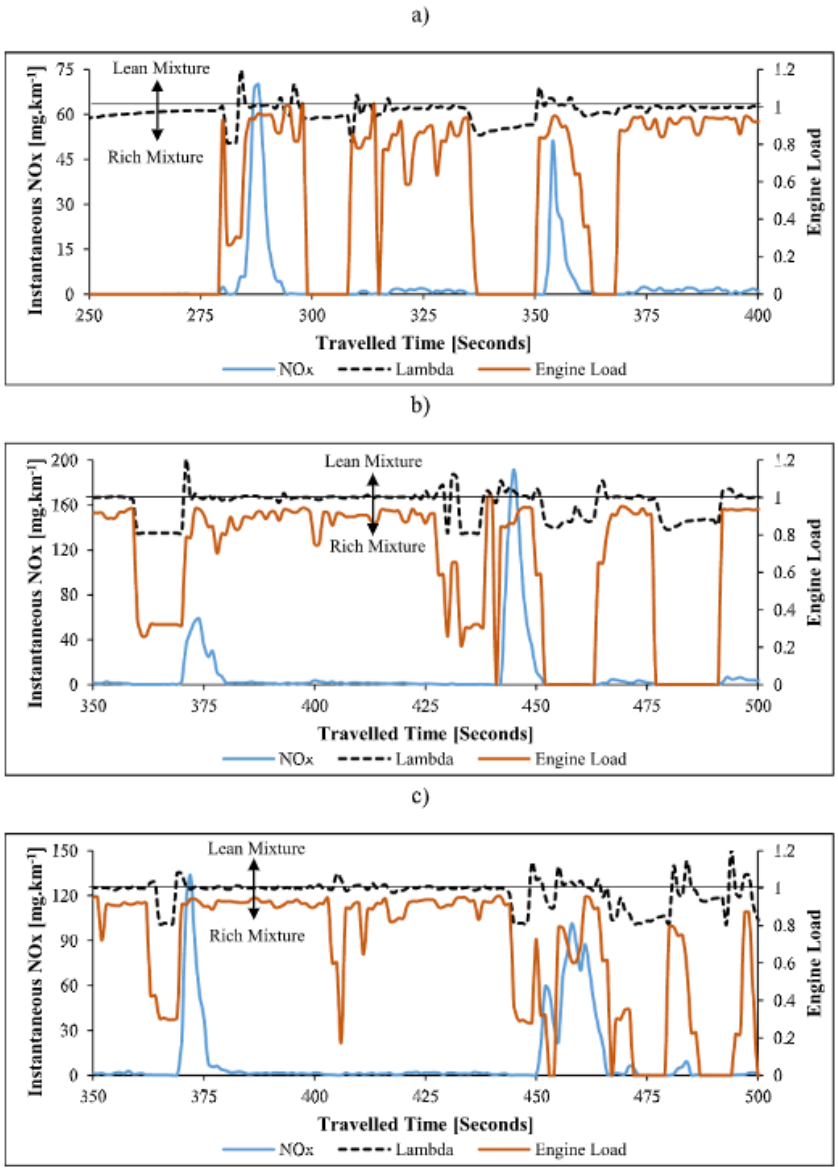

Fig. 5. Effect of engine restart on instantaneous NOx emissions: a) R1; b) R2; and c) R3. Note: Engine Load is expressed in decimal values.

4.2. Engine on/off operation rules

An important aspect of developing an emissions model for HEVs is that the pollutant emissions must be differentiated based on whether the ICE is “on” or “off”, in addition to parameters, such as vehicle speed and acceleration. ICE is typically “off” during idling mode, decelerations and cruise modes under low speed, and during positive accelerations at low speed, which can be interpreted as combinations of low accelerations with low to moderate speeds, or as moderate accelerations with low speeds [13]. Since HEV operates in ICE “on” most of the time, there is a need for developing a practical approach for estimating HEVs emission rates to avoid the use of the ICE in partial loads regimes. On the other hand, an emission characterization based on a well-defined ICE status operation can result in more reliable predictions of HEVs emission rates.

Engine speed is an indicator of engine "on" or "off" operation [13]. As soon as an engine starts, the engine speed is usually around 600–1000 RPM during idling [42], [43]. Selecting a conservative approach, 500 RPM was used as the threshold value, below which the ICE status is ''off'' [13]. It must be emphasized that the ICE status threshold may not be perfectly accurate when characterizing the ICE status between "on" and "off", which may result in data corresponding to ICE status "on" being analyzed as if the ICE status was "off". PEMS usually detects the remaining exhaust pollutants flowing out through the exhaust tailpipe during a few proceeding instants even in low engine speed values.

To test the applicability of the proposed RPM threshold value, Table 4 summarizes the average values of FFR, CO_2, NOx and PM in both ICE operation modes. The results indicated that, regardless of the route type, fuel consumption and emissions were near zero, thus confirming 500 RPM as a suitable threshold to categorize ICE as "on" and "off". With these concerns in mind, the developed models based on ICE "on" data consider zero emission rates for engine speed values lower than 500 RPM.

Table 4. Summary of cycle average FFR, CO_2, NOx, and PM.

Engine	Route	FFR (l. h^{-1})	CO_2 (g. s^{-1})	NOx (mg. s^{-1})	PM (mg. s^{-1})
RPM < 500	R1	0.147	0.036	0.001	0.002
	R2	0.130	0.042	0.001	0.002
	R3	0.190	0.046	0.007	0.002
RPM > 500	R1	4.033	1.781	0.088	0.030
	R2	8.539	4.500	0.172	0.059
	R3	7.294	3.739	0.082	0.052

Note: Values represent all measurements.

4.3. Exploratory data analysis

Analysis of variance (ANOVA) statistical test was used to explore the significance of the effect of variation in dependent variables (route type, speed interval and vehicular jerk) on variation in measured emission rates and ICE engine state. The null hypothesis of the test is that the emission mean values among route types (R1, R2 and R3), speed intervals (s1, s2 and s3), and jerk types (1–9) are equal at a significance level of 5%. For this comparison, speed values were divided into three main intervals: s1 ≤ 50 $km.h^{-1}$; 50 < s2 ≤ 90 $km.h^{-1}$; s3 > 90 $km.h^{-1}$.

Table 5 lists ANOVA results performed for the ICE "on" and ICE "off" datasets. For CO_2, speed and jerk type variables were found to be significant in explaining the variability in the mean emission rates in ICE status "off", whereas for NOx, a significant correlation was only found when using route type as the input variable. For PM, only speed and jerk type explained the variability in the mean emission rates. It must be stressed that almost all data corresponding to engine speeds lower than 500 RPM had, although very low, positive emissions rates for NOx and PM (about 30% of PEMS raw data is characterized by zero-value emission rates for RPM < 500), thereby justifying why the input variables were able to significantly explain the variability in the mean emission rates during the ICE "off" operation. Route type and speed interval were typically significant factors in explaining the variability in the mean emission rates during ICE status "on" (p-value < 0.05, and thus mean values are not equal). The reported p-values also confirmed that jerk type was useful in explaining the variability in the mean emission rates, but these were higher for PM than for CO_2 and NOx. Jerk type was thus found as an appropriate explanatory variable to be applied in the development of emissions models of this hybrid car.

Table 5. ANOVA results (p-value) for emission rates with respect to route type, speed, and jerk type by ICE status.

ANOVA results (p-value) for emission rates with respect to route type, speed, and jerk type by ICE status.

Condition	Input Variable	CO_2	NO_X	PM
ICE "off"	Route Type	0.466	< 0.001	0.573
	Speed	< 0.001	0.164	< 0.001
	Jerk Type	< 0.001	0.988	0.006
ICE "on"	Route Type	< 0.001	< 0.001	< 0.001
	Speed	< 0.001	< 0.001	< 0.001
	Jerk Type	0.031	0.039	< 0.001

Note: Values lower than 0.05 indicate statistically significant at significance level.

To fully understand group differences in prior ANOVA, multiple pairwise tests between routes (Table S10), speed intervals (Table S11) and jerk types (Table S12) were conducted. For each pollutant and ICE operation status, and based on pairwise comparisons, R1 emission rates were found to be statistically significant in relation to the R2 and R3 at a 5% significance level. R2 and R3 did not exhibit statistically significance for CO_2 and NOx during ICE "off" operation, and for NOx and PM during ICE "on" operation, which can be explained by the similar driving conditions of these routes. The analysis of pairwise comparisons between speed intervals revealed that s2 and s3 emission rates were not statistically significant in ICE "off", which is expected since electric motor usually works at low speeds. The analysis of jerk resulted in a statistically significance found in the jerk types comprising between 2–5, 2–7, and 2–9, and in jerk types comprising between 3–5, 3–6, and 3–9, when ICE was "on". For the remaining cases, the multiple pairwise analysis did not detect statistically significance at a 5% significance level. This can be due to a fewer number of occurrences in some jerk types. Thus, a dataset was created from all trips to analyze emission rates by jerk type.

4.4. Estimation emission model based in driving volatility

Fig. 6a show the time distribution by jerk type of all the combined ICE on/off dataset while Fig. 6b contains stacked columns with percentage of time with ICE "on" and "off" in each jerk type. It must be stated that driving volatility-based models were calibrated using 70% of the trips [44]. Fig. 6a allows to conclude that cruise state (type 9) represented 28% of the combined ICE on/off dataset and that jerk types 2, 3, 5, and 6 also represented appreciable amounts of operation in the range of ~16–19%. In contrast, the proportion of alternate accelerating and decelerating (types 7 and 8), and uniform acceleration (type 1) and deceleration (type 4) accounted for about 1% of the driving time. The frequency of each jerk type ranging from 1 to 3 in ICE status "on" was over 73% of the driving time, while between jerk types 4 and 7, more than 40% of the driving time are defined as belonging to ICE status "off", as depicted in Fig. 6b. This latter result is reasonable because driving behavior for types 4, 5, and 6 represents two consecutive instants of deceleration during which the electric motor is restoring energy while providing power to the auxiliary systems, and thus less or no fuel injections is expected.

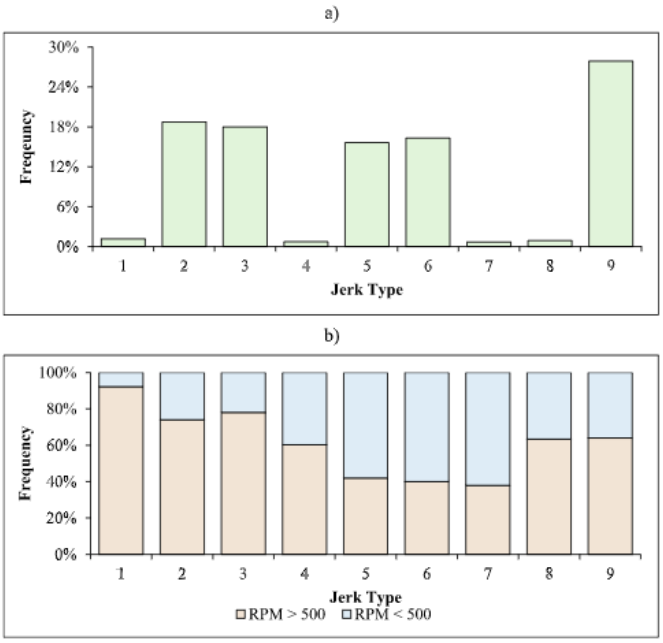

Fig. 6. Time distribution by jerk type using the training dataset: a) percentage of time using all ICE on/off data; and b) percentage of time using separated ICE on/off data.

4.4.1. Cruise state

It must be mentioned that speed cannot represent, per se, the HEV mass emissions during a cruise state. The analysis of experimental data confirmed that the instantaneous emission rate was often different at the same cruise speed and equal at different cruise speeds (see Figs. S14 to S16). For instance, values encompassing all the range of the engine speeds were found for vehicle speeds of 50 $km.h^{-1}$, 70 $km.h^{-1}$ or 100 $km.h^{-1}$. Thus, E_{cruise} was represented as a function of engine speed instead.

Fig. 7 examines the relationship between CO_2, NOx and PM emission rates and RPM. The coefficient of determination (R^2) values for CO_2 and PM applying quadratic polynomial functions of RPM were higher than 0.90 regardless of the ICE operation rules. The p-values for both linear and quadratic parameters were less than 0.05, indicating statistical significance. The scatter plots show a cluster of data with low emission rates between 500 RPM and 2000 RPM that might be associated with electric mode operation for short periods (2–3 s). Since NOx formation depends on combustion flame temperature, and is therefore less sensitive to variations in engine speed, the fit between NOx and RPM was worse than those obtained for CO_2 or PM. To improve NOx predictions when the vehicle is in a cruise condition, data for emissions higher than 0.2 $mg.s^{-1}$ were disregarded when developing the models, which represents less than 10% of data (but approximately 35% of total NOx emissions). The fitted equation for emission rates versus RPM can be given by:

$$m'_{CO2,\,ICEon/off} = 7.55\times10^{-4}RPM + 4.77\times10^{-7}RPM^2 \;(R^2 = 0.94, Fsig < 0.05) \quad (5)$$

$$m'_{CO2,\,ICEon} = 8.79\times10^{-4}RPM + 4.33\times10^{-7}RPM^2 \;(R^2 = 0.96, Fsig < 0.05) \quad (6)$$

$$m'_{NOx,\,ICEon/off} = 1.10\times10^{-5}RPM + 2.26\times10^{-9}RPM^2 \;(R^2 = 0.55, Fsig < 0.05) \quad (7)$$

$$m'_{NOx,\,ICEon} = 1.21\times10^{-5}RPM + 1.86\times10^{-9}RPM^2 \;(R^2 = 0.57, Fsig < 0.05) \quad (8)$$

$$m'_{PM,\,ICEon/off} = 6.30\times10^{-6}RPM + 6.17\times10^{-9}RPM^2 \;(R^2 = 0.91, Fsig < 0.05) \quad (9)$$

$$m'_{PM,\,ICEon} = 6.44\times10^{-6}RPM + 6.12\times10^{-9}RPM^2 \;(R^2 = 0.92, Fsig < 0.05) \quad (10)$$

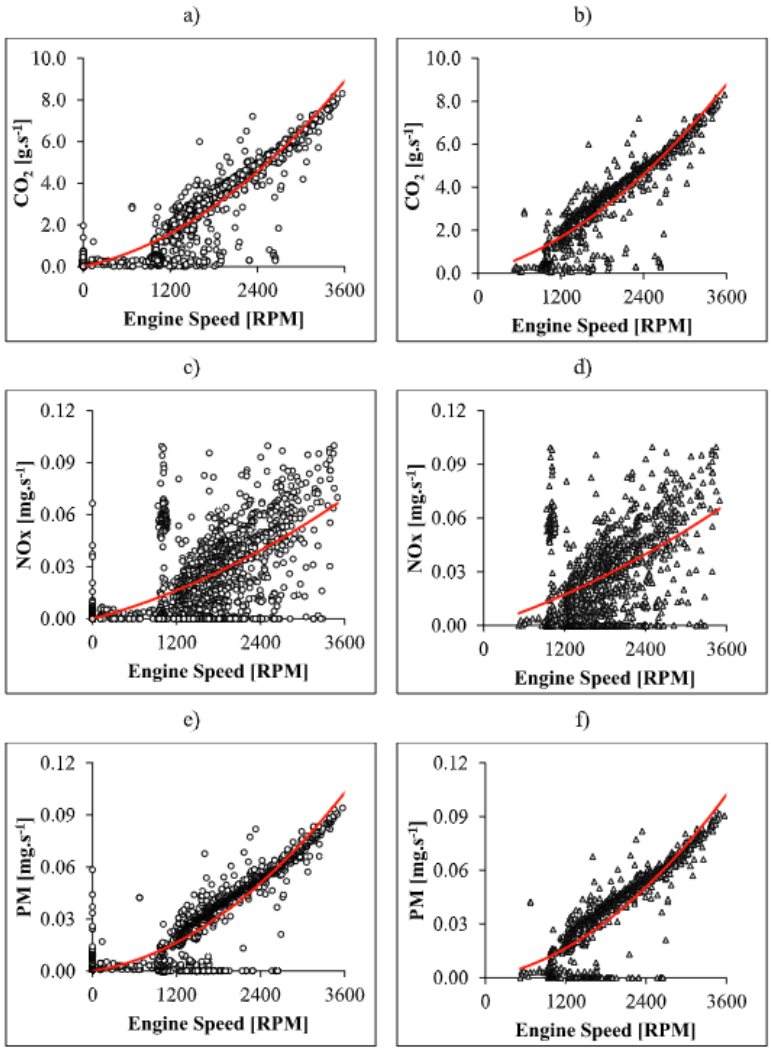

Fig. 7. Speed counter map for cruise state: a) RPM versus CO_2 with ICE on/off data; b) RPM versus CO_2 with ICE on data; c) RPM versus NOx with ICE on/off data; d) RPM versus NOx with ICE on data; e) RPM versus PM with ICE on/off data; and f) RPM versus PM with ICE on data.

4.4.2. Volatile state

Similar to the cruise conditions, HEV emission rates in volatile states were predicted based on engine speed. Fig. 8 illustrates the relationship between CO_2 emission rates and RPM for volatile states (jerk type 1–8) considering both ICE on/off data. The data was analyzed considering the vehicle as a black box without distinction between ICE and electric operation. The fitting functions of jerks 4 and 5 were similar such that one equation was used to represent both of these types. This assumption is in line with previous research conducted by Zhang et al. [29]. It is worth noticing that these models represent deceleration episodes for those jerks that are equal or higher than 0 $m.s^{-3}$. Concerning the remaining jerk types, the scatter plots revealed that most of the data points followed a polynomial function (R^2 values using a quadratic polynomial of RPM ranged from 0.77 to 0.94, depending on the jerk type). Statistical significance (p-values < 0.05) was also confirmed in both linear and quadratic parameters. The fitting curves for NOx and PM by jerk type are exhibited in Fig. S17 and Fig. S18, respectively. The predictive emission models for volatile types and considering both ICE on/off data are as follows:

$$m'_{CO2,\ \text{ICE on/off}} = \begin{cases} \text{if jerk type} = 1,\ 9.12\times10^{-4}RPM + 4.08\times10^{-7}RPM^2 (R^2 = 0.94,\ Fsig < 0.05), \\ \text{if jerk type} = 2,\ 7.86\times10^{-4}RPM + 4.36\times10^{-7}RPM^2 (R^2 = 0.92,\ Fsig < 0.05), \\ \text{if jerk type} = 3,\ 6.83\times10^{-4}RPM + 4.69\times10^{-7}RPM^2 (R^2 = 0.92,\ Fsig < 0.05), \\ \text{if jerk types} = 4,5,\ 2.69\times10^{-4}RPM + 6.53\times10^{-7}RPM^2 (R^2 = 0.84,\ Fsig < 0.05), \\ \text{if jerk type} = 6,\ 2.57\times10^{-4}RPM + 6.49\times10^{-7}RPM^2 (R^2 = 0.83,\ Fsig < 0.05), \\ \text{if jerk type} = 7,\ 1.99\times10^{-4}RPM + 7.18\times10^{-7}RPM^2 (R^2 = 0.90,\ Fsig < 0.05), \\ \text{if jerk type} = 8,\ -2.15\times10^{-4}RPM + 6.63\times10^{-7}RPM^2 (R^2 = 0.77,\ Fsig < 0.05), \end{cases} \tag{11}$$

$$m'_{NOx,\ \text{ICE on/off}} = \begin{cases} \text{if jerk type} = 1,\ 3.46\times10^{-6}RPM + 6.98\times10^{-9}RPM^2 (R^2 = 0.50,\ Fsig < 0.05), \\ \text{if jerk type} = 2,\ 1.83\times10^{-5}RPM + 6.40\times10^{-11}RPM^2 (R^2 = 0.42,\ Fsig < 0.05), \\ \text{if jerk type} = 3,\ 1.55\times10^{-5}RPM + 1.05\times10^{-9}RPM^2 (R^2 = 0.41,\ Fsig < 0.05), \\ \text{if jerk types} = 4,5,\ 4.25\times10^{-5}RPM - 6.95\times10^{-9}RPM^2 (R^2 = 0.35,\ Fsig < 0.05), \\ \text{if jerk type} = 6,\ 4.31\times10^{-5}RPM - 7.59\times10^{-9}RPM^2 (R^2 = 0.35,\ Fsig < 0.05), \\ \text{if jerk type} = 7,\ 2.95\times10^{-5}RPM - 6.31\times10^{-9}RPM^2 (R^2 = 0.35,\ Fsig < 0.05), \\ \text{if jerk type} = 8,\ 1.85\times10^{-5}RPM - 3.99\times10^{-9}RPM^2 (R^2 = 0.25,\ Fsig < 0.05), \end{cases} \tag{12}$$

$$m'_{PM,\ \text{ICE on/off}} = \begin{cases} \text{if jerk type} = 1,\ 9.95\times10^{-6}RPM + 4.80\times10^{-9}RPM^2 (R^2 = 0.94,\ Fsig < 0.05), \\ \text{if jerk type} = 2,\ 8.45\times10^{-6}RPM + 5.38\times10^{-9}RPM^2 (R^2 = 0.85,\ Fsig < 0.05), \\ \text{if jerk type} = 3,\ 8.99\times10^{-6}RPM + 5.37\times10^{-9}RPM^2 (R^2 = 0.81,\ Fsig < 0.05), \\ \text{if jerk types} = 4,5,\ 2.03\times10^{-6}RPM + 7.77\times10^{-9}RPM^2 (R^2 = 0.79,\ Fsig < 0.05), \\ \text{if jerk type} = 6,\ 3.70\times10^{-6}RPM + 7.20\times10^{-9}RPM^2 (R^2 = 0.76,\ Fsig < 0.05), \\ \text{if jerk type} = 7,\ 2.63\times10^{-6}RPM + 7.83\times10^{-9}RPM^2 (R^2 = 0.88,\ Fsig < 0.05), \\ \text{if jerk type} = 8,\ 4.03\times10^{-6}RPM + 6.92\times10^{-9}RPM^2 (R^2 = 0.86,\ Fsig < 0.05), \end{cases} \tag{13}$$

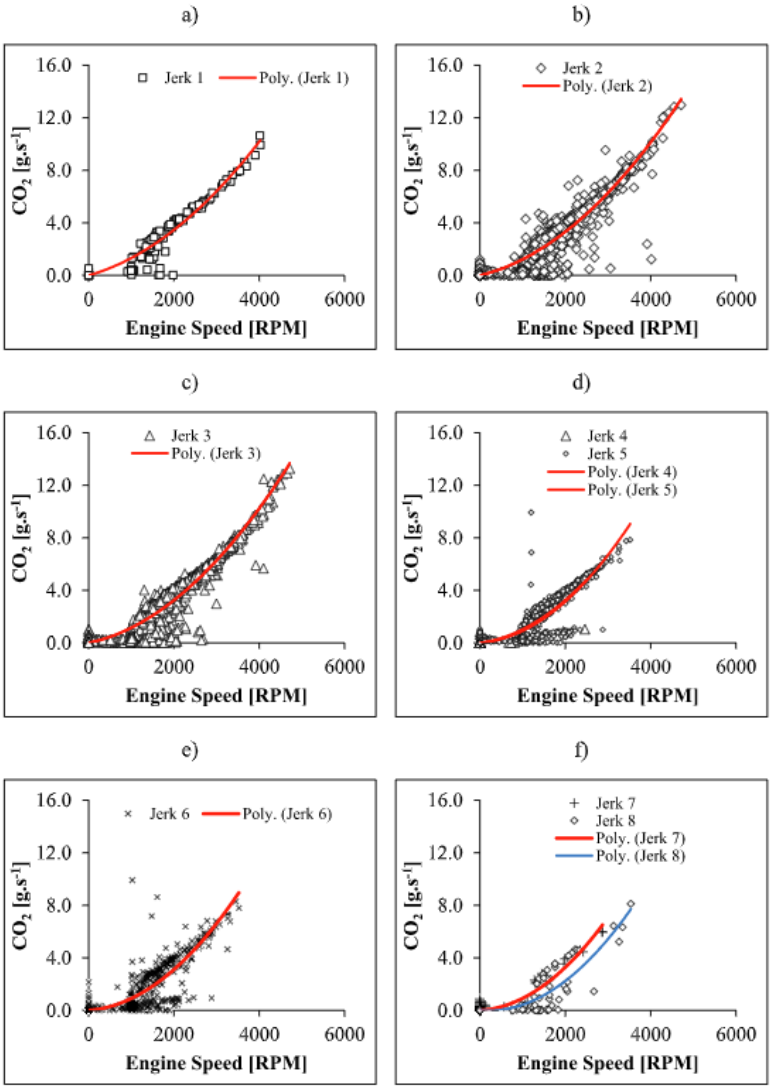

Fig. 8. Relationship between CO_2 and RPM considering both ICE on/off data: a) jerk type 1; b) jerk type 2; c) jerk type 3; d) jerk types 4 and 5; e) jerk type 6; and f) jerk types 7 and 8.

Fig. 9 depicts CO_2 emission rates predictions versus each volatile jerk type for ICE status "on" data. Most CO_2 data, ranging from 0 to nearly 13 $g.s^{-1}$, followed a polynomial quadratic trend versus RPM. The R^2 values were between 0.78 and 0.93 for jerk types 8 and 1, respectively. The results for PM also showed R^2 values of 0.72 or higher between predicted and measured emission rates. However, the analysis of fitting curves for NOx by jerk type did not identify a correlation between RPM and emissions using only engine speed data higher than 500 RPM, as shown in Fig. S19. So, the prediction of NOx for volatile states was based on Equation (12). For CO_2 and PM (see Fig. S20), the fitted models are as follows:

$$\dot{m}'_{CO2,\ ICE\ on} = \begin{cases} \text{if jerk type} = 1,\ 9.14\times10^{-4}RPM + 4.07\times10^{-7}RPM^2\ (R^2 = 0.93,\ Fsig < 0.05), \\ \text{if jerk type} = 2,\ 7.88\times10^{-4}RPM + 4.36\times10^{-7}RPM^2\ (R^2 = 0.92,\ Fsig < 0.05), \\ \text{if jerk type} = 3,\ 6.86\times10^{-4}RPM + 4.69\times10^{-7}RPM^2\ (R^2 = 0.92,\ Fsig < 0.05), \\ \text{if jerk types} = 4,5,\ 2.65\times10^{-4}RPM + 6.55\times10^{-7}RPM^2\ (R^2 = 0.83,\ Fsig < 0.05), \\ \text{if jerk type} = 6,\ 2.54\times10^{-4}RPM + 6.50\times10^{-7}RPM^2\ (R^2 = 0.83,\ Fsig < 0.05), \\ \text{if jerk type} = 7,\ 1.87\times10^{-4}RPM + 7.24\times10^{-7}RPM^2\ (R^2 = 0.89,\ Fsig < 0.05), \\ \text{if jerk type} = 8,\ -2.59\times10^{-4}RPM + 6.89\times10^{-7}RPM^2\ (R^2 = 0.78,\ Fsig < 0.05), \end{cases} \quad (14)$$

$$\dot{m}'_{PM,\ ICE\ on} = \begin{cases} \text{if jerk type} = 1,\ 9.95\times10^{-6}RPM + 4.80\times10^{-9}RPM^2\ (R^2 = 0.94,\ Fsig < 0.05), \\ \text{if jerk type} = 2,\ 8.43\times10^{-6}RPM + 5.38\times10^{-9}RPM^2\ (R^2 = 0.88,\ Fsig < 0.05), \\ \text{if jerk type} = 3,\ 8.99\times10^{-6}RPM + 5.37\times10^{-9}RPM^2\ (R^2 = 0.81,\ Fsig < 0.05), \\ \text{if jerk types} = 4,5,\ 1.96\times10^{-6}RPM + 7.81\times10^{-9}RPM^2\ (R^2 = 0.80,\ Fsig < 0.05), \\ \text{if jerk type} = 6,\ 3.66\times10^{-6}RPM + 7.22\times10^{-9}RPM^2\ (R^2 = 0.77,\ Fsig < 0.05), \\ \text{if jerk type} = 7,\ 2.49\times10^{-6}RPM + 7.89\times10^{-9}RPM^2\ (R^2 = 0.89,\ Fsig < 0.05), \\ \text{if jerk type} = 8,\ 2.25\times10^{-5}RPM + 5.12\times10^{-9}RPM^2\ (R^2 = 0.72,\ Fsig < 0.05), \end{cases} \quad (15)$$

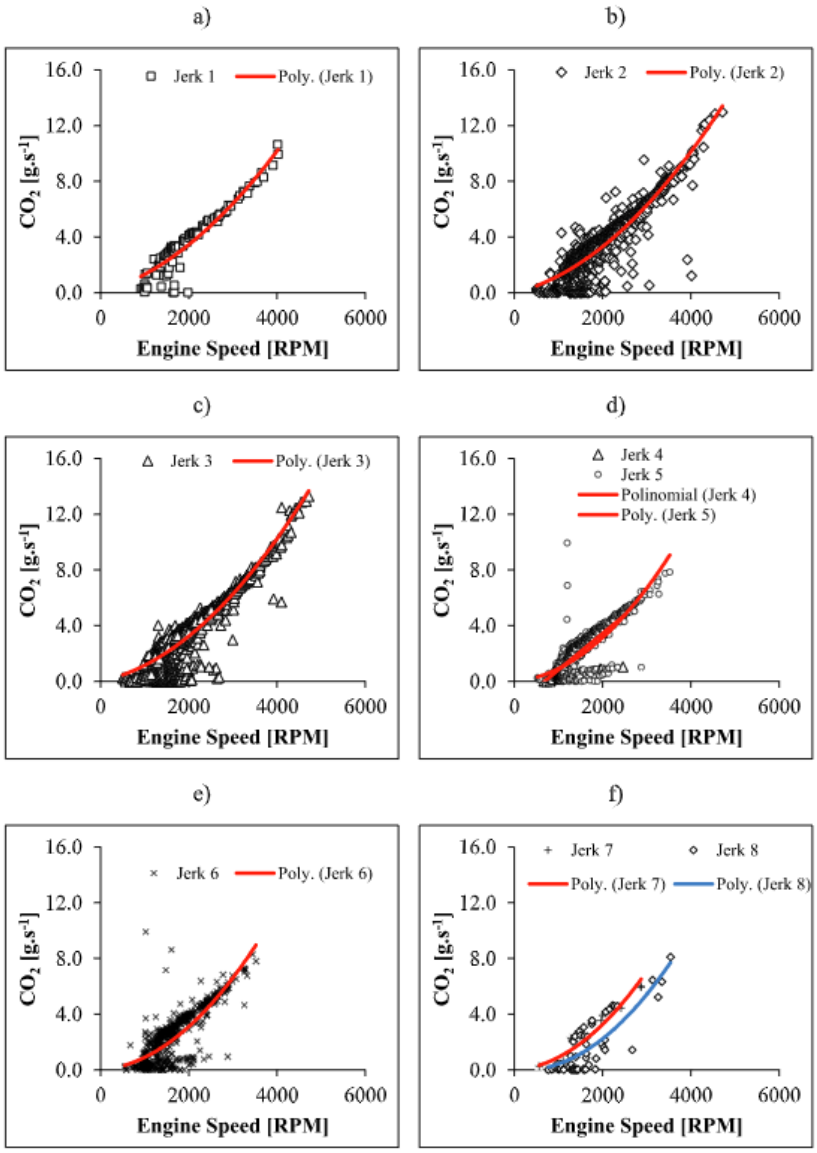

Fig. 9. Relationship between CO_2 and RPM considering ICE on data: a) jerk type 1; b) jerk type 2; c) jerk type 3; d) jerk types 4 and 5; e) jerk type 6; and f) jerk types 7 and 8.

4.4.3. Validation of the jerk-based models

To assess the goodness of fit, measured and estimated emission rates were compared using testing data. Table 6 summarizes the coefficients of determination between jerk types estimated emission rates and measured emission rates by ICE operation rules, shown by pollutant. R^2 values of RPM versus CO_2 emission rates were 0.64 or higher, considering both ICE on/off data. If only engine speed data higher than 500 RPM were used, then R^2 values between estimated and measured emission rates would be 0.59 or higher. For NOx, R^2 values for the driving-volatility based models ranged from 0.04 to 0.35, indicating a poor fit. This is due to the fact that NOx concentrations were below the instrument detection limit for approximately 47% of the data, which in turn led to random variability in the data [34]. The results for PM were generally good in jerk types associated with cruise speed (9), and alternate positive and negative accelerations (7–8), with R^2 values ranging from 0.70 and 0.93, considering both ICE on/off data. Driving volatility-based models established for ICE "on" data had R^2 values higher than 0.60 for both CO_2 and PM. Overall, in terms of R^2, the models based on jerk behavior, and using RPM as explanatory variable showed robustness in estimating HEV CO_2 and PM emission rates, regardless of the ICE operation rules.

Table 6. Coefficients of determination for ICE on/off versus ICE "on" for emission rates.

Jerk Type	CO_2		NO_X		PM	
	ICE on/off versus measured	ICE on versus measured	ICE on/off versus measured	ICE on versus measured[a]	ICE on/off versus measured	ICE on versus measured
1	0.95	0.92	0.35	–	0.87	0.87
2	0.91	0.88	0.13	–	0.66	0.61
3	0.89	0.85	0.16	–	0.80	0.80
4 and 5	0.90	0.81	0.24	–	0.61	0.75
6	0.87	0.75	0.13	–	0.84	0.78
7	0.93	0.90	0.04	–	0.91	0.93
8	0.64	0.59	0.08	–	0.70	0.84
9	0.94	0.87	0.21	0.22	0.93	0.78

Note: No models were developed for jerk types 1 to 8 using ICE status "on" data.

4.5. Performance comparison with VSP model

To complement the analysis, the performance of the proposed driving volatility-based models was compared against the VSP-modal approach [45]. The vehicle specific power (or the instantaneous force required to overcome all road loads) is a useful exploratory variable for HEV emissions [16], [13]. Thus, second by-second speed, acceleration and slope road data (using training set) were grouped in 14 modes, where each mode is associated with an emission factor of CO_2, NOx and PM (see Table S2 and Fig. S21 for full details). After that, emissions for four trips from the testing data were computed using the developed ICE on/off and ICE "on" models, and VSP, and then compared against field values.

Table 7 summarizes trip information and the CO_2, NOx, and PM predictions for each model per unit distance. The results showed that driving volatility-based models' ability to estimate CO_2 emissions was acceptably accurate when compared to field values, especially for the ICE "on" model; the differences ranged from 1% to 16%, depending on the trip. A comparison with VSP confirmed that driving volatility-based models resulted in better CO_2 predictions. For instance, the differences between VSP using ICE "on" data and measured values ranged from 7% to 25%, depending on the trip. The analysis of NOx estimates also confirmed that the proposed models were aligned with VSP for almost all trips. However, the VSP-modal approach resulted in a higher overestimation of field NOx (8–15 times on average) than the driving volatility-based approach (2–3 times on average). Concerning PM, the VSP model appeared to predict similar values to field data (up to 29%) for different types of routes using ICE "on" data. The driving volatility-based models underpredicted the average PM per unit distance for both ICE operation rules (on average 25% less than the field trip values).

Table 7. Summary of the trip emission prediction results by model.

Trip ID	Type	CO_2 [g.km^{-1}]					NOx [mg.km^{-1}]					PM [mg.km^{-1}]				
		Field[a]	VSP		Driving Volatility		Field[a]	VSP		Driving Volatility		Field[a]	VSP		Driving Volatility	
			ICE on/ off	ICE on	ICE on/ off	ICE on		ICE on/ off	ICE on	ICE on/ off	ICE on		ICE on/ off	ICE on	ICE on/ off	ICE on
1	R1	130	101	139	130	139	0.52	4.17	4.30	1.36	1.12	1.06	1.32	1.34	1.29	1.28
2	R2	55	102	67	57	56	0.23	5.86	3.54	0.70	0.59	1.31	1.47	0.93	0.58	0.56
3	R1	65	117	81	76	75	0.28	6.92	4.20	0.95	0.90	1.06	1.68	1.13	0.77	0.76
4	R3	72	112	90	77	76	0.55	6.10	4.50	0.97	0.91	1.11	1.59	1.25	0.76	0.75
Average		80	108	94	85	84	0.40	5.76	4.13	0.99	0.88	1.14	1.51	1.16	0.85	0.85

Note: Measured value that corresponds to the sum of emission rates for each pollutant (CO_2, NOx, and PM) along each trip (testing set) and divided by the total distance.

The performance analysis of the CO_2 driving volatility-based models with the prominent VSP model also resulted in a better fit based on the root mean square error (RMSE) metric on each trip (Table S13). Although models based on VSP and driving volatility achieved different trip-specific NOx and PM values in both ICE operation rules, RSME values were identical between trips.

5. Conclusions and future work

A method using real-world emissions and engine data to estimate hybrid electric vehicle emissions rates as a function of driving volatility was demonstrated. The modeling approach can be used by applying vehicle activity, engine and emissions data when hybrid electric vehicle operation is considered as a ‘‘black box” and a well-defined internal combustion engine status on and off is acquired.

The results indicated that the vehicular jerk is a good explanatory variable in estimating emission rates. Time fraction estimates for both internal combustion engine status “on” and internal combustion engine on and off data for all jerk types agreed well with training data. Also, driving volatility-based models based on engine RPM showed a good fit in predicting both CO_2 (R^2 between 0.77 and 0.96, depending on the jerk type) and particulate matter (R^2 between 0.72 and 0.99, depending on the jerk type) emission rates using quadratic polynomial regression analysis, but they were worse in predicting nitrogen oxides emissions (R^2 values were 0.57 or less). For NOx emissions, this was mostly explained by the proportion of the measured concentrations lower than the instrument detection limit (~47%), which resulted in random variability. Driving volatility-based models yielded similar CO_2 and particulate matter compared to measured values for different route types, and lower error values than a vehicle specific power-modal approach.

This research can contribute to assessing transportation-related energy and emissions impacts through the definition of driving behavior based on vehicle acceleration and jerk types that represent different driving regimes. The proposed driving volatility-based models can be integrated into the electronic car unit to inform drivers about specific spikes in instantaneous emissions rates associated to volatile driving. Although there are different types of hybrids with different kick starts for the internal combustion engine and resultant emission impacts, the methodology developed in this research can be applied in other hybrid electric vehicles and conventional internal combustion engine vehicles with different engine speed ranges and torques. This can be done via the following steps: 1) obtain acceleration and jerk, engine speed and internal combustion engine status; 2) classify jerk type 1–9 based on acceleration and vehicular jerk; and 3) establish a relationship between engine speed and emission rates by jerk type. The use of driving volatility information can be useful to achieve more energy efficient driving behavior control systems for all autonomous vehicles, and in particular, for vehicles powered by hybrid electric technology.

The engine speed threshold value applied to categorize internal combustion engine status was a conservative value that may not be in full accordance with this vehicle operation. The use of an engine speed threshold to define internal combustion engine on/off was less robust when predicting residual emissions between 500 and 2000 RPM which are associated with electric mode operation during deceleration episodes (2–3 s). The driving volatility-based models developed in this research did not take into account specific spikes in nitrogen oxides emission rates, which can represent a large fraction in total emissions for certain jerk types, since they were determined to be rare events.

ICE and exhaust emissions data measured using PEMS in additional models of HEVs are needed to examine the variability in engine on/off rules and emission rates and provide higher robustness to the models. Emission rates were measured with a particular PEMS, but additional data from other vehicles can be measured either using a similar PEMS or other available equipment in the market. There is the potential to augment model performance by incorporating other Internally Observable Variables (e.g., torque, engine load or manifold absolute pressure), testing speed modal approaches, and using stratified emission data (e.g., NOx or PM). Future steps are the possibility of collecting real-time engine and activity information using connected vehicle technologies that can improve the relationship between driving volatility and HEVs, and between HEVs and road traffic systems. The definition of warning systems concerning instantaneous driver behaviors using recommended jerk and emission thresholds to define volatile driving should also be explored.

Credit authorship contribution statement

P. Fernandes: Conceptualization, Methodology, Validation, Formal analysis, Investigation, Data curation, Writing - original draft, Visualization, Writing - review & editing. R. Tomás: Conceptualization, Methodology, Validation, Formal analysis, Data curation, Visualization, Writing - review & editing. E. Ferreira: Conceptualization, Formal analysis, Data curation, Writing - review & editing. B. Bahmankhah: Investigation, Resources, Writing - review & editing. M.C. Coelho: Writing - review & editing, Supervision, Project administration, Funding acquisition.

Declaration of Competing Interest

The authors declare that they have no known competing financial interests or personal relationships that could have appeared to influence the work reported in this paper.

Acknowledgements

This work was supported by the projects UIDB/00481/2020 and UIDP/00481/2020 - FCT - Fundação para a Ciência e a Tecnologia; and CENTRO-01-0145-FEDER-022083 - Centro Portugal Regional Operational Programme (Centro2020), under the PORTUGAL 2020 Partnership Agreement, through the European Regional Development Fund; MobiWise (P2020 SAICTPAC/0011/2015), co-funded by COMPETE2020, Portugal2020 - Operational Program for Competitiveness and Internationalization (POCI), European Union's ERDF (European Regional Development Fund), and FCT; DICA-VE (POCI-01-0145-FEDER-029463) project funded by FEDER through COMPETE2020, and by national funds (OE), through FCT/MCTES. Finally, the cooperation of Toyota Caetano Auto S.A. is appreciated, which allowed the use of HEV for data collection.

Appendix A. Supplementary material

Supplementary data to this article can be found online at https://doi.org/10.1016/j.apenergy.2020.116250.

References

[1] EEA. The first and last mile — the key to sustainable urban transport. Transport and environment report 2019, European Environmental Agency, Copenhagen, Denmark, Available from

https://www.eea.europa.eu/publications/the-first-and-last-mile/the-first-and-last-mile/viewfile#pdfjs.action=download; 2019.

[2] EEA. Air quality in Europe — 2019 report. EEA Report No 10/20192019.

[3] EC. Regulation (EC) No 443/2009 of the European Parliament and of the Council of 23 April 2009 setting emission performance standards for new passenger cars as part of the Community's integrated approach to reduce CO2 emissions from light-duty vehicles. In: http://data.europa.eu/eli/reg/2009/443/2018-05-17, editor. Official Journal of the European Union; 2009:1402009.

[4] EEA. Average carbon dioxide emissions from new passenger cars, Available from: https://www.eea.europa.eu/data-and-maps/daviz/average-emissions-for-new-cars-5#tab-googlechartid_chart_11; 2019.

[5] ACEA. New passenger car registrations in the EU by alternative fuel type, European Automobile Manufacturers' Association, Brussels, Belgium, Available from https://www.acea.be/uploads/press_releases_files/20190206_PRPC_fuel_Q4_2019_FINAL.pdf. 2020.

[6] IEA. Global EV Outlook 2019 - Scaling-up the transition to electric mobility. International Energy Agency; 2019.

[7] L.K. Mitropoulos, P.D. Prevedouros, P. Kopelias Total cost of ownership and externalities of conventional, hybrid and electric vehicle. Transp Res Procedia, 24 (2017), pp. 267-274

[8] C. Mi, M.A. Masrur. Hybrid electric vehicles: principles and applications with practical perspectives. Wiley (2017)

[9] E. Ericsson. Independent driving pattern factors and their influence on fuel-use and exhaust emission factors. Transport Res Part D: Trans Environ., 6 (2001), pp. 325-345

[10] Y. Wang, C. Hao, Y. Ge, L. Hao, J. Tan, X. Wang, et al. Fuel consumption and emission performance from light-duty conventional/hybrid-electric vehicles over different cycles and real driving tests Fuel, 278 (2020), Article 118340

[11] W. Zhuang, S. Li, X. Zhang, D. Kum, Z. Song, G. Yin, et al. A survey of powertrain configuration studies on hybrid electric vehicles. Appl Energy, 262 (2020), Article 114553

[12] T. Younglove, G. Scora, M. Barth. Designing on-road vehicle test programs for the development of effective vehicle emission models. Transp Res Rec, 1941 (2005), pp. 51-59

[13] H. Zhai, H. Christopher Frey, N.M. Rouphail. Development of a modal emissions model for a hybrid electric vehicle. Transport Res Part D: Trans Environ, 16 (2011), pp. 444-450

[14] R. Alvarez, M. Weilenmann. Effect of low ambient temperature on fuel consumption and pollutant and CO2 emissions of hybrid electric vehicles in real-world conditions. Fuel, 97 (2012), pp. 119-124

[15] R. Alvarez, P. Schlienger, M. Weilenmann. Effect of hybrid system battery performance on determining CO2 emissions of hybrid electric vehicles in real-world conditions. Energy Policy., 38 (2010), pp. 6919-6925

[16] G.O. Duarte, R.A. Varella, G.A. Gonçalves, T.L. Farias. Effect of battery state of charge on fuel use and pollutant emissions of a full hybrid electric light duty vehicle. J Power Sources, 246 (2014), pp. 377-386

[17] B.A. Holmén, K.M. Sentoff. Hybrid-electric passenger car carbon dioxide and fuel consumption benefits based on real-world driving. Environ Sci Technol, 49 (2015), pp. 10199-10208

[18] X. Wu, S. Zhang, Y. Wu, Z. Li, W. Ke, L. Fu, et al. On–road measurement of gaseous emissions and fuel consumption for two hybrid electric vehicles in Macao. Atmos Pollut Res, 6 (2015), pp. 858-866

[19] Y. Huang, N.C. Surawski, B. Organ, J.L. Zhou, O.H.H. Tang, E.F.C. Chan. Fuel consumption and emissions performance under real driving: Comparison between hybrid and conventional vehicles. Sci Total Environ, 659 (2019), pp. 275-282

[20] M. Conger, B.A. Holmén. Characterization of real-world particle number emissions during reignition events from a 2010 light-duty hybrid electric vehicle. Transp Res Rec, 2503 (2015), pp. 137-146

[21] H.C. Frey, X. Zheng, J. Hu. Variability in measured real-world operational energy use and emission rates of a plug-in hybrid electric vehicle. Energies, 13 (2020).

[22] M.K. Robinson, B.A. Holmén. Hybrid-electric passenger car energy utilization and emissions: Relationships for real-world driving conditions that account for road grade. Sci Total Environ, 738 (2020), Article 139692

[23] J. Liu, A. Khattak, X. Wang. A comparative study of driving performance in metropolitan regions using large-scale vehicle trajectory data: Implications for sustainable cities. Int J Sustain Transport, 11 (2017), pp. 170-185

[24] G. Fontaras, P. Pistikopoulos, Z. Samaras. Experimental evaluation of hybrid vehicle fuel economy and pollutant emissions over real-world simulation driving cycles. Atmos Environ, 42 (2008), pp. 4023-4035

[25] M.C. Coelho, M.B. Luzia. Evaluating the energy performance of a SUV hybrid electric vehicle. Transport Res Part D: Trans Environ, 15 (2010), pp. 443-450

[26] J. Liu, X. Wang, A. Khattak. Customizing driving cycles to support vehicle purchase and use decisions: Fuel economy estimation for alternative fuel vehicle users. Transport Res Part C: Emerg Technol, 67 (2016), pp. 280-298

[27] J. Rios-Torres, J. Liu, A. Khattak. Fuel consumption for various driving styles in conventional and hybrid electric vehicles: Integrating driving cycle predictions with fuel consumption optimization. Int J Sustain Transport, 13 (2019), pp. 123-137

[28] B. Bahmankhah, P. Fernandes, J. Teixeira, M.C. Coelho. Interaction between motor vehicles and bicycles at two-lane roundabouts: a driving volatility-based analysis. Int J Injury Control Safety Promotion, 26 (2019), pp. 205-215

[29] Zhang L, Zhao X, Khattak A. A new fuel consumption model considering vehicle's speed, acceleration and jerk. In Presented at the 99th Transportation Research Board Annual Meeting, 12-16 January. Washington D.C., U.S.; 2020.

[30] P Fernandes, R Tomas, F Acuto, A Pascale, B Bahmankhah, C Guarnaccia, et al. Impacts of roundabouts in suburban areas on congestion-specific vehicle speed profiles, pollutant and noise emissions: An empirical analysis. Sustainable Cities and Society, 62 (2020), p. 102386

[31] P. Fernandes, E. Macedo, B. Bahmankhah, R.F. Tomas, J.M. Bandeira, M.C. Coelho. Are internally observable vehicle data good predictors of vehicle emissions? Transport Res Part D: Trans Environ, 77 (2019), pp. 252-270

[32] P. Fernandes, M. Vilaça, E. Macedo, C. Sampaio, B. Bahmankhah, J.M. Bandeira, et al. Integrating road traffic externalities through a sustainability indicator. Sci Total Environ, 691 (2019), pp. 483-498

[33] 3DATX. http://www.3datx.com/. 3-dimensional data analysis (3DATX) Corporation; 2018.

[34] G. Sandhu, H. Frey. Effects of errors on vehicle emission rates from portable emissions measurement systems. Transport Res Record: J Transport Res Board., 2340 (2013), pp. 10-19

[35] B. Yazdani Boroujeni, H.C. Frey. Road grade quantification based on global positioning system data obtained from real-world vehicle fuel use and emissions measurements. Atmos Environ, 85 (2014), pp. 179-186

[36] EC. Commission Regulation (EU) 2017/1151 of 1 June 2017 supplementing Regulation (EC) No. 715/2007 of the European Parliament and of the Council on type-approval ofmotor vehicles with respect to emissions fromlight passenger and commercial vehicles (Euro 5 and Euro 6) and on access to vehicle repair andmaintenance information, amending Directive 2007/46/EC of the European Parliament and of the Council, Commission Regulation (EC) No. 692/2008 and Commission Regulation (EU) No. 1230/2012 and repealing Commission Regulation (EC) No. 692/2008. Official Journal of the European Union. 2017:643.

[37] M. Delavarrafiee, H.C. Frey. Real-world fuel use and gaseous emission rates for flex fuel vehicles operated on E85 versus gasoline. J Air Waste Manage Assoc, 68 (2018), pp. 235-254

[38] EPA. Title 40 - Protection of Environment, Section 86.144-94 - Calculations; exhaust emissions. United States Environmental Protection Agency, Retrieved from: https://www.govinfo.gov/content/pkg/CFR-2012-title40-vol19/xml/CFR-2012-title40-vol19-sec86-144-94.xml, Accessed date: 7 July 2019 2018.

[39] Charles Fayette T. Combustion in diesel engines. Internal Combustion Engine in Theory and Practice: Combustion, Fuels, Materials, Design: MITP; 1985. p. 1.

[40] M.C. Coelho, H.C. Frey, N.M. Rouphail, H. Zhai, L. Pelkmans. Assessing methods for comparing emissions from gasoline and diesel light-duty vehicles based on microscale measurements. Transport Res Part D: Trans Environ, 14 (2009), pp. 91-99

[41] Lin W, Sterniak J, Bohac SV. NOx emissions characterization during transient spark assisted compression ignition (SACI) engine operation. ASME 2013 Internal Combustion Engine Division Fall Technical Conference. Dearborn, MI; 2013.

[42] Ribbens WB. Chapter 6 - Digital Powertrain Control Systems. In: Ribbens WB, editor. Understanding Automotive Electronics (Eighth Edition): Butterworth-Heinemann; 2017. p. 271–341.

[43] N. Sharma, P.V.P. Kumar, R. Dhyani, C. Ravisekhar, K. Ravinder. Idling fuel consumption and emissions of air pollutants at selected signalized intersections in Delhi. J Cleaner Prod, 212 (2019), pp. 8-21

[44] H. Liu, A. Gegov, M. Cocea. Unified Framework for Control of Machine Learning Tasks Towards Effective and Efficient Processing of Big Data. W. Pedrycz, S.-.M. Chen (Eds.), Data Science and Big Data: An Environment of Computational Intelligence, Springer International Publishing, Cham (2017), pp. 123-140

[45] USEPA. Methodology for developing modal emission rates for EPA's multi-scale motor vehicle & equipment emission system. Ann Arbor, MI: Prepared by North Carolina State University for US Environmental Protection Agency; 286 p. Report No.: EPA420-R-02-0272002.